Adsorption of Indigo Carmine Dye onto Physicochemical-Activated Leaves of *Agave Americana* L

Ben Nasr, Jalel*[+]

Electromechanical Systems Laboratory LASEM, National Engineering School of Sfax, University of Sfax, Soukra km 4, 3038 Sfax, TUNISIA

Ghorbal, Achraf[•]

Research Laboratory LR18ES33, National Engineering School of Gabes, University of Gabes, Rue Omar ibn el Khattab 6072 Gabes, TUNISIA

ABSTRACT: *Dyes represent a serious threat to the environment when released in wastewaters. Hence, the main objective of this work was to design and fabricate an activated carbon from an invasive plant – Agave Americana L – capable of removing indigo carmine in aqueous solutions. The equilibrium adsorption of indigo carmine was assessed using the Freundlich, Langmuir, and Dubinin-Radushkevich isotherm model. The zinc chloride was used to activate the powder of Agave at 600 °C and 900 °C. The results of this work showed that the elaborated activated carbon had maximum adsorption of 61.72 mg/g and a specific surface area of 38 m²/g determined using the BET method. The thermodynamic study showed that the adsorption of indigo carmine on the activated carbon was endothermic. Therefore, the activated carbon prepared from the Agave Americana L would be an efficient and cost-effective alternative adsorbent of indigo carmine and would have a positive effect on the environment.*

KEYWORDS: *Agave Americana L; Activated carbon; Adsorption; Indigo Carmine*.

INTRODUCTION

Indigo carmine, one of the frequently used dyes in industries of textile, food, leathers, plastic, and paper, was unanimously considered as one of the main pollutants of the environment [1–5]. More specifically, *Mufrettin* [2] argued that the toxicity of this dye causes skin and eye irritation and permanent injury to the cornea and conjunctiva to human being. Moreover, *Mufrettin* [2] and *Lakshmi et al.* [6] revealed that indigo carmine causes problems respiratory illnesses as coughing and shortness of breath. For these reasons, researchers worked on developing ways of removing this dye from wastewaters. One of the suggested methods was adsorption [7,8]. The main adsorbent used

* *To whom correspondence should be addressed.*

+ *E-mail: jalelbennasr@yahoo.fr*

● *Other Address: Higher Institute of Applied Sciences and Technology of Gabes, university of Gabes, Rue Omar ibn el Khattab 6072 Gabes, TUNISIA*

1021-9986/2021/4/1054-1066 13/$/6.03

was the activated carbon (AC). This material was obtained from the conversion of some industrial by-products in order to valorize them and to reduce some environmental problems [9-13]. In parallel, activated carbon was produced from invasive plants and algae [14], and agricultural and wood wastes [15] such as sugar cane bagasse [16], Jatoba fruit barks [17], walnut shell, hazelnut shell, almond shell, and pistachio shell [18].

However, despite the advantages attributed to the use of these materials as substitutes for commercial activated carbon, they still suffer from some hindrances for their extensive processing. The activated carbon properties depend on the activation conditions methods, the chemical activation, the physio-chemical activation, and the physical activation [19,20]. Indeed, several scholars observed that such adsorbents were operational only where dye concentrations exceeded 200 mg/L and could only remove 50 mg/g. In addition, it was reported that their AC needed specific preparation and could be used only as a targeted adsorbent. Nevertheless, to our knowledge, nobody has investigated the *Agave Americana L* (Fig.1) as a source of AC. This plant was characterized by *Mansouri et al.* [21] and *Bezazi et al.* [22]. It was praised for its cheap production in the Mediterranean area, its large-sized and rigid leaves an important cellulose percentage.

For these reasons, the main objective of this study was to explore the possibility of producing AC from *Agave Americana L* to remove the Indigo Carmine (IC) dye (Fig.2) from wastewaters. Furthermore, the study intended to focus on the determination of the specific surface area and the pore volume of the AC. Our ultimate objective was to alleviate the polluting effects of wastewaters and valorize abundant but so far useless *Agave Americana L* plants and thus produce an AC at a reduced cost.

EXPERIMENTAL SECTION

Preparation of activated carbon

The dry leaves were collected from a natural plantation of *Agave Americana L* in the area of Sousse, Tunisia. The leaves were washed with distilled water and dried for 24 h at 120 °C. After that, the leaves were crushed; the obtained grain size varied between 100 µm and 600 µm. The method adopted in this preparation was the chemical and physical activation. The detailed preparation conditions were conducted as was reported in previous works [15]. The *Agave Americana L* with a size range

Fig. 1: A natural plantation of Agave Americana L from the area of Sousse, Tunisia.

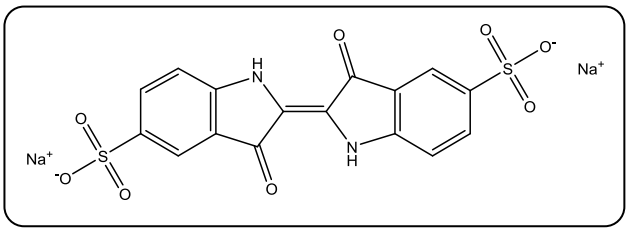

Fig. 2: Chemical structure of Indigo Carmine (IC).

between 100 µm and 600 µm were used. The $ZnCl_2$ was dissolved in distilled water, then impregnated into the Agave for a ratio of chloride zinc ranging from 1 to 1.5. The mixture was dried in an oven at 110 °C. The Agave impregnated $ZnCl_2$ was fired in flowing dry N_2 at a heating rate of 10 °C/min. After activation, the products were washed sufficiently with de-ionized water. The activation temperatures were 600 and 900 °C at a heating rate of 10 °C/min with an introduction of wet N_2 for 2 hours.

Indigo carmine dye

Adsorption of IC on activated carbon was studied in the different solutions of dyes at different conditions. Table 1 exhibits some of IC properties.

Batch experiments

The granulometry of the AC used in this study was 20 µm. This study adopted batch adsorption. It was conducted in 100 mL Erlenmeyer flasks. Each flask contained 50 mL of IC solution. The solution pH was adjusted by adding a solution of sodium hydroxide (0.1 N NaOH) or Hydrochloric acid (0.1 N HCl). The amount of adsorbed dye onto AC was determined by measuring the difference between initial and final dye concentrations,

Table 1: Indigo Carmine dye properties.

Dyestuff	Indigo Carmine
Empirical formula	$C_{16}H_8N_2Na_2O_8S_2$
IUPAC name	disodium;2-(3-hydroxy-5-sulfonato-1*H*-indol-2-yl)-3-oxoindole-5-sulfonate
Melting point	300 °C
Charges in aqueous solution	Negative
Solubility in water at 25 °C	10 g/L
Density	1.35
UV max	608 nm in water

using a spectrophotometer. The wavelength of IC absorbance was 608 nm. All the experiments were triplicated. The following conditions were adopted for the experiments: an IC concentration ranging between 20 and 200 mg/L, a contact time ranging between 2 and 45 min, and adsorbent dosage of 40 mg, an adsorbate phase pH ranging between 2 and 11, a temperature of 25, 35, and 45 °C and a stirring speed of 150 rpm.

The adsorption capacity q_e (mg/g) was computed following equation (1):

$$q_e = (C_0 - C_e)\frac{V}{M} \quad (1)$$

Where C_0 (mg/L) is the initial concentration, $\mathbf{C_e}$ (mg/L) is the equilibrium concentration of IC, V is the volume of solution (L) and M is the mass of AC (g).

Fourier Transformation InfraRed (FT-IR)

The infrared spectra were obtained by a Spectrum Two (PerkinElmer, USA) spectrophotometer using a Pyroelectric Deuterated Glycine Sulfate (DTGS) detector. An Attenuated Total Reflection (ATR) attachment with a diamond crystal was used. Measurements were performed in the 450–4000 cm^{-1} wavenumber range with a resolution of 2 cm^{-1}.

Scanning Electron Microscopy (SEM)

The microscopy observations were obtained by Scanning Electron Microscopy (SEM) technique. A JSM-540 (JEOL LTD, Japan) was used to observe the microstructure of the AC.

RESULTS AND DISCUSSION

Chemical composition of the Agave Americana L

The determination of the chemical composition was conducted following ASTM standard protocols. Samples were first submitted to reflux extraction with ethanol/toluene (ASTM D 1107-56) and water (ASTM 1110-56). The chemical contents were determined using the following methods: lignin (ASTM D 1106-56), cellulose (ASTM D 1104-56), α-cellulose (ASTM D 1103-60) and ash (ASTM D 1102-84) [23]. The *Agave Americana L* consisted of cellulose, hemicellulose, lignin, pectin, and ash. The results of chemical composition are represented in Table 2.

FT-IR analysis

The FT-IR spectrum exhibited in Fig. (3a) revealed that the *Agave Americana L* was a complex lignocellulosic material with three major constituents: cellulose, hemicellulose, and lignin [24,25]. The 3320 cm^{-1} strong absorption band would be attributed to hydroxyl group vibrations [26,27]. The band at 2917 cm^{-1} would correspond to the C-H stretching in cellulose and hemicelluloses [28]. The vibration at 2852 cm^{-1} would be attributed to the C-H stretching in lignin and waxes. The strong band at 1032 cm^{-1} would be due to C–O, C=C, and C–C–O vibrational stretches of the *Agave Americana L* cellulose, hemicellulose, and lignin [29].

Characterization of the activated carbon

Fig. 3 shows the FT-IR spectra of the *Agave Americana L* and the corresponding AC. After the activation procedure and the thermal degradation, several bands located in the spectrum of the *Agave Americana L* disappeared (Fig. 3b). Indeed, the combination of high temperature and the presence of the activating agent caused the partial and/or the complete destruction of many functional groups. For instance, the disappearance and/or the sharp intensity decrease of bands at the 2600–3600 cm^{-1} range would indicate the removal of hydroxyl groups from the material structure after the activation process [30].

Table 2: Chemical composition of the Agave Americana L.

Elements	Cellulose	Hemicellulose	Lignin	Pectin	Ash
%	60.50	15	5.75	5	13.75

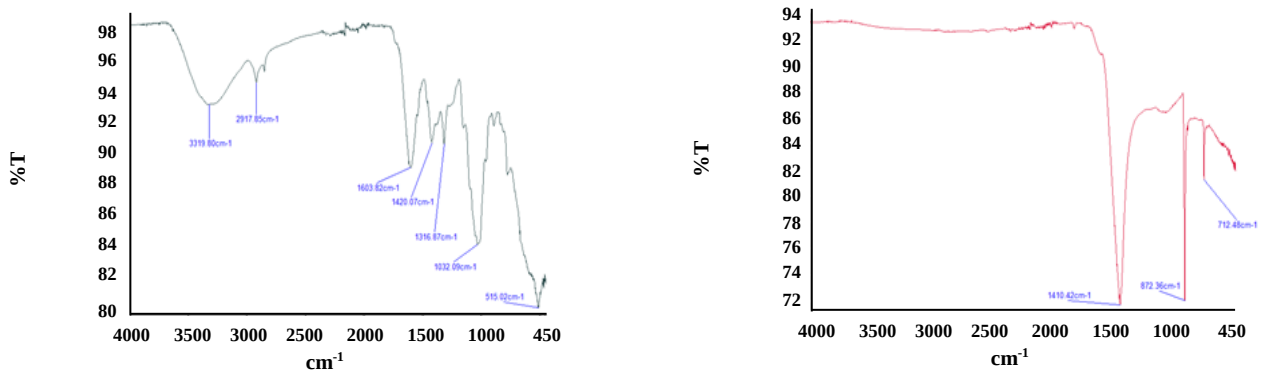

Fig. 3: FT-IR spectra of the Agave Americana L (a) and Agave Americana L based activated carbon (b).

The high temperature together with the activating agent broke many bonds thus leading to partial and/or complete destruction of most surface functional groups. The C–H out-of-plane bending in benzene derivatives was commonly found on the surface of various activated carbons. In line with *Sahraei et al.* [1] and *Ahmed et al.* [31], this study revealed a significant sharp decrease in the band intensities in the bandwidths of 1700–3500 cm^{-1} as the hydroxyl group disappeared

SEM analysis of activated carbon

Scanning electron microscopy (SEM) images of crushed *Agave Americana L* fibers and $ZnCl_2$-activated carbon (AC900) and (AC600) are shown in Fig. 4. The comparison of these images shows that the thermal and chemical modification significantly changed the morphology of the *Agave Americana L* powder surface. Indeed, the raw powder surface seemed planar, without any pores (Fig. 4a). However, the AC surface seemed to have many porous structures (Fig. 4b) and (Fig. 4c), indicating that cavities were developed during the chemical activation. Indeed, *Pezoti Junior et al.* [32] and *Deng et al.* [33] explained that the pore structure was related to the evaporation of the activating reagent $ZnCl_2$ during the activation process.

Characterization of specific surface area and pore volume of activated carbon

Table 3 shows *Agave Americana L* AC adsorption capacity. The Brunauer Emmett Teller (BET) surface areas

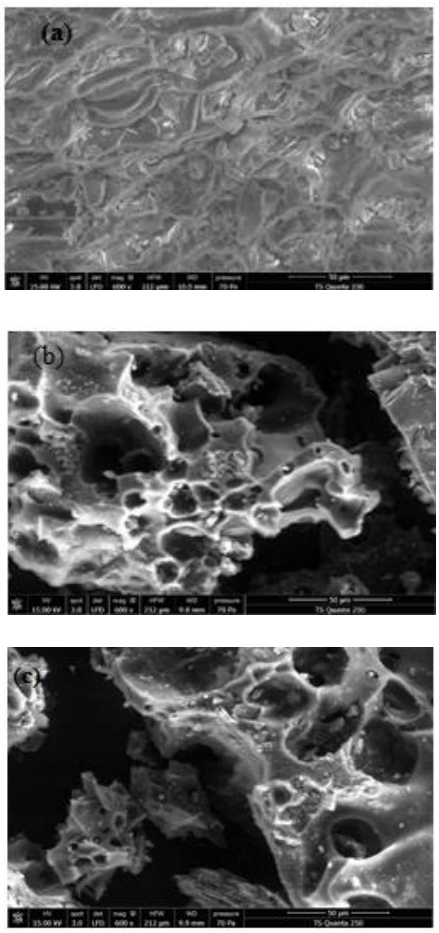

Fig. 4: (a) SEM images of crushed Agave Americana L fibers, (b) Activated carbon (AC900), (c) Activated carbon (AC600).

Table 3: Surface area and pore volume of AC600 and AC900.

Surface area	AC600	AC900	Unit
Single point surface area at p/p° = 0.194135232	129.797	185.020	m^2/g
BET(*) Surface Area	128.056	183.040	m^2/g
Pore Volume			
Single point adsorption total pore volume of pores less than 7.022 Å diameter at p/p° = 0.000955028	0.0223	0.0523	cm^3/g
BJH(**)= Adsorption cumulative volume of pores between 17.000 Å and 3000.000 Å diameter	0.04878	0.0753	cm^3/g
BJH(**) Desorption cumulative volume of pores between 17.000 Å and 3000.000 Å diameter	0.04183	0.07118	cm^3/g

(*) BET: Brunauer Emmett Teller; (**) BJH: Barrett Joyner Halenda

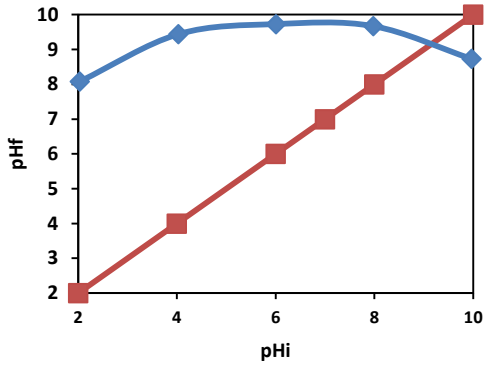

Fig. 5: Determination of pH_{pzc} of AC prepared from the Agave Americana L.

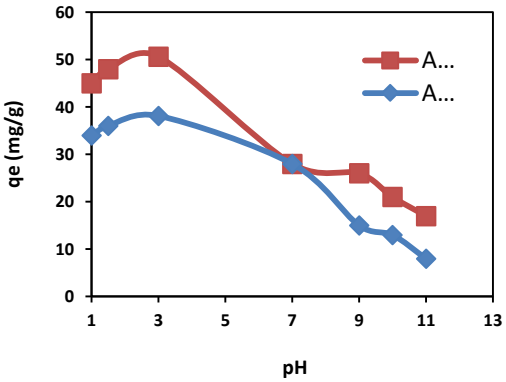

Fig. 6: Effect of pH on adsorption of IC on the AC 600 and AC900 (T = 25 °C, C_0 = 50 mg/L, Contact time = 20 min).

of AC at 600 °C and AC at 900 °C were 128 and 183 m^2/g, respectively. The Barrett Joyner Halenda (BJH) method revealed that the total pore volumes for AC600 and AC900 were 0.075 and 0.049 cm^3/g, respectively. Therefore, the nitrogen adsorption/desorption isotherms and pore volume measurement would represent clear evidence that AC600 and AC900 have porous structures. Furthermore, this finding would prove that the surface area sorption capacity was enhanced.

Determination of pH_{pzc}

As was already reported by [6,34], pH point of zero charge measurements pH_{pzc} is defined as the pH of an aqueous solution in which the AC exists under neutral electrical potential. As can be seen in Fig. 5, the pH_{pzc} was equal to 9. When pH is less than pH_{pzc}, the AC surface is positively charged and the removal of anions is favored. However, if pH is greater than pH_{pzc}, the surface is negatively charged and uptake of cations by the sorbent is favored [29].

The effect of pH on the adsorption of Indigo Carmine

Fig. 6 shows the effect of pH on the adsorption of IC on the AC600 and AC900 at 25 °C after a contact time of 20 min IC amounts adsorbed per mass unit by AC600 and AC900 prepared from *Agave Americana L*, at 600 °C and 900 °C, respectively. The maximum adsorption was obtained at acid pH equal to 3. In this pH range the IC was positively charged ($-H^+$) and the surface of activated carbon was negatively charged. The deprotonated groups of activated carbon were mainly the carboxylic group ($-CO-O^-$) and phenolic ($-O^-$). With a pH solution equal to 3, the removal capacity of IC was expected to increase as the adsorbent was negatively charged and dye molecules were positively charged. As was explained by several authors [6,24,25,29], the constant adsorption capacity of AC for dyes was an indication that the electrostatic mechanism was not the only mechanism for dye adsorption in this system.

The effect of contact time on the amount of the adsorbed IC at the optimum pH

Fig. 7 shows the effect of contact time on the adsorption of

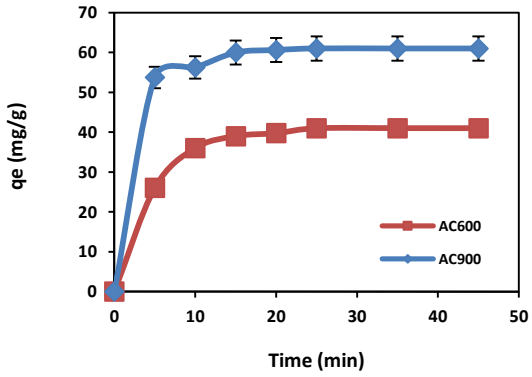

Fig. 7: The effect of contact time on the adsorption of IC on AC600 and AC900 (pH = 3.0, T = 25 °C, C_0 = 50 mg/L).

Fig. 7: The effect of contact time on the adsorption of IC on AC600 and AC900 (pH = 3.0, T = 25 °C, C_0 = 50 mg/L).

IC on AC600 and AC900 at 25 °C. The contact time required for the adsorbent-adsorbate system to reach the state of equilibrium was termed the equilibrium time.

The amount of dye adsorbed at the equilibrium time was equal to the maximum adsorption capacity of the adsorbent under those operating conditions. It can be seen that most of IC adsorption on the AC600 and AC900 attained equilibrium conditions in 15 min where the concentration of dye ions in the solution was in dynamic balance with that at the interface [35,36].

Adsorption kinetics

the Kinetic modeling allows the estimation of sorption rates. Hence it may lead to suitable rate expressions characteristic of possible reaction mechanisms. In this context, three kinetics were tested, the pseudo-first-order (Eq. (2)), pseudo-second equation (Eq. (3)), and Elovich model (Eq. (4)).

Pseudo-first order model

The pseudo-first-order equation is given by

$$ln(q_e - q_t) = lnq_e - k_1 t \quad (2)$$

Where q_e and q_t are the amounts of IC adsorbed (mg/g) at equilibrium and time t (min), respectively, and $k_1$is the rate of constant adsorption (min^{-1}). The value of k_1 was calculated from the plots of $ln(q_e-q_t)$ in relation to t shown in Fig. 8. k_1=0.0567 and k_1= 0.049 for AC600 and AC900, respectively. The experimental q_e values differed from the calculated ones, obtained from the linear plots. This would show that the adsorption of IC on to AC600 and AC900 was not a first-order kinetic.

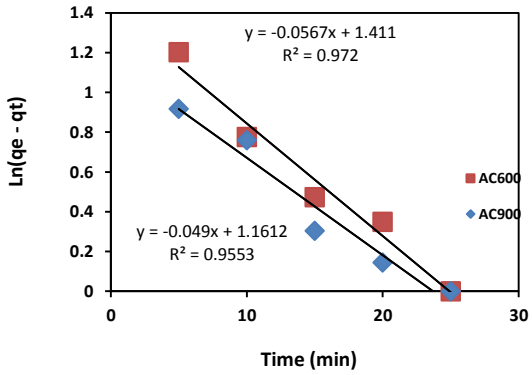

Pseudo-second-order model

The pseudo-second-order is defined by

$$\frac{t}{q_t} = \frac{1}{k_2 q_e^2} + \frac{t}{q_e} \quad (3)$$

where k_2 (g/mg min) is the constant rate of second-order adsorption. The condition of applying this model is that the plot of t/q in the function of t should show a linear relationship. There is no need to know any parameter beforehand and q_e and k_2 can be determined from the slope and the intersection of the plot. In addition, this procedure is more likely to predict the behavior over the whole range of adsorption. The linear plots of t/q in the function of t (Fig. 9) show a good agreement between experimental and calculated adsorption capacity values. The correlation coefficients for the second-order kinetic model were R^2 = 0.9971 and R^2 = 0.9996 for AC600 and AC900, respectively. These values were greater than 0.99, indicating the applicability of the second-order and thus representing a good model of the adsorption process of IC on AC600 and AC900.

Elovich kinetic model

The Elovich model [30] is defined by

$$q_e = \frac{1}{\beta}\ln(\alpha\beta) + \frac{1}{\beta}\ln(t) \quad (4)$$

Where α represents the initial sorption rate (mg/g min) and β represents the desorption constant (g/mg), the Elovich coefficient α and β were calculated from the plot of qe vs ln(t) (Fig. 10). The correlation coefficients for the Elovich kinetic model were R^2 = 0.8127 and R^2 = 0.8519 for AC600 and AC900, respectively. These values were less than 0.9, indicating that the Elovich model was not applicable in the adsorption process of IC on AC600 and AC900.

Table 4: Comparison of the pseudo-first-order, pseudo-second-order, and Elovich models for AC600 and AC900.

Materials	Pseudo-first-order				Pseudo-second-order			Elovich model		
	q_{exp} (mg/g)	q_{th} (mg/g)	k (min^{-1})	R^2	q_{th} (mg/g)	K (g/mg min)	R^2	α (mg/g min)	β (g/mg)	R^2
AC600	42	4.100	0.056	0.972	46.169	0.005	0.997	52.826	0.066	0.812
AC900	62	3.193	0.049	0.955	63.694	0.015	0.999	3175.575	0.122	0.851

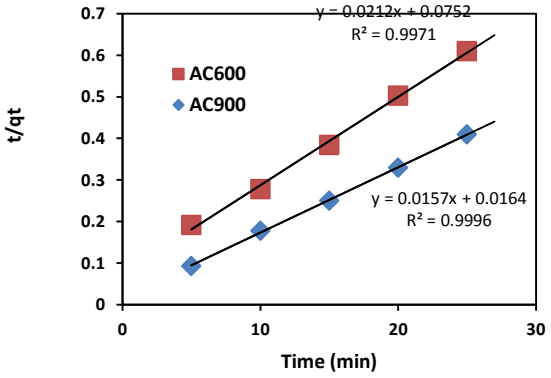

Fig. 9: Pseudo second-order kinetic plots for adsorption of IC on AC600 and AC900 (pH=3.0, T= 25 °C, C_0=50 mg/L).

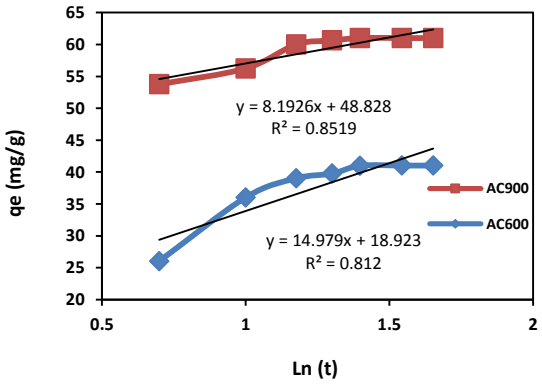

Fig. 10: Elovich model plots for adsorption of IC on AC600 and AC900 (pH=3.0, T= 25 °C, C_0=50 mg/L).

The parameters obtained for the pseudo-first-order, pseudo-second-order models, and Elovich model for AC600 and AC900 are presented in Table 4.

The interaction between dye and adsorbent

Fig. 11 shows the equilibrium isotherms of IC dye on the AC600 and the AC900. This work revealed that there was an interaction between the dye molecule and an adsorbent molecule when the adsorption process reached the equilibrium phase.

The adsorption isotherm was defined by two models: Langmuir and Freundlich. The Freundlich isotherm model assumes heterogeneous surface energies, in which the energy term in the Langmuir equation varies as a function of the surface coverage. The Langmuir isotherm showed monolayer adsorption onto a surface containing a well-defined number of adsorption sites. The correlation coefficient R^2 was an important factor to compare the applicability of the isotherm model.

The Langmuir isotherm model is given in Equation (5)

$$\frac{C_e}{q_e} = \frac{1}{q_0 b} + \frac{1}{q_0} C_0 \qquad (5)$$

Where q_e is the amount of adsorbate adsorbed per unit mass of adsorbate (mg/g): C_e is the equilibrium concentration of the adsorbate IC (mg/L); $q_0$and b are Langmuir constants related to the rate of adsorption and adsorption capacity, respectively. Fig.12 shows C_e/q_e plotted against C_e. The graph shows a straight line with a slope $1/q_0$. Therefore, it can be inferred that the adsorption of IC on AC900 and AC600 followed the Langmuir isotherm. The Langmuir constants 'b' and 'q_0' which were calculated from this isotherm are given in Table 5.

The experimental results revealed that the isothermal model of Langmuir was adequate for the study of adsorption isotherm. This model proved that the activated carbon surfaces were homogenous. Moreover, this finding confirms previous results by *Malik* [37], and Namasivayam and Kavitha [38] stating that there was a monolayer cover of IC molecules on the external surface of the AC. The dimensionless equilibrium parameter of the Langmuir isotherm (R_l) is defined by Eq. (6).

$$R_L = \frac{1}{1+bC_0} \qquad (6)$$

Where C_0 is the highest dye concentration (50 mg/L) and *b* was the Langmuir constant. The type of the isotherm depends on the values of R_L. Therefore, it would be

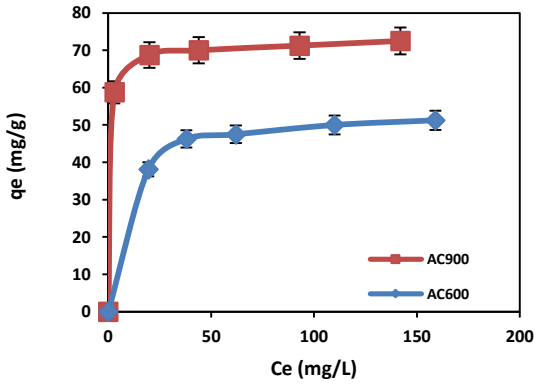

Fig. 11: Equilibrium isotherms of IC on AC600 and AC900 (pH=3.0, T= 25 °C, contact time = 20 min).

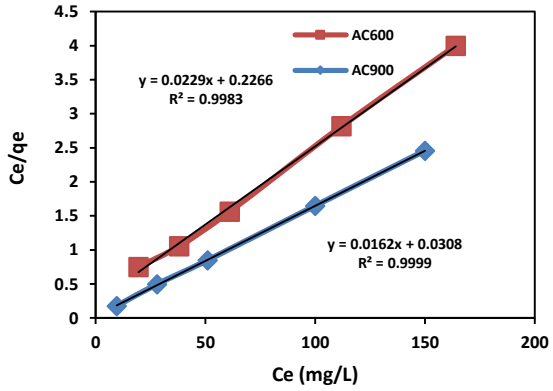

Fig. 12: Langmuir isotherm model for removal of IC by AC600 and AC900 (pH=3.0, T= 25 °C, C_0=50 mg/L).

unfavorable for (R_L>1) or linear for (R_L=1) or favorable for (0<R_L<1) or irreversible for (R_L=0). In this study, R_L was equal to 0.166 for the adsorption of AC600 and R_L was equal to 0.030 for the AC900. This value would prove that the two solids were favorable for the adsorption of IC under the conditions used in this study.

The Freundlich model is given by equation (7):

$$lnq_e = lnk_f + \frac{1}{n} lnC_e \quad (7)$$

Where C_e is the equilibrium concentration of the adsorbate; q_e is the amount adsorbed at equilibrium (mg/g); n and k_f are Freundlich constants; k_f is the adsorption capacity of the adsorbent and n indicates the intensity of adsorption. k_f represents the quantity of dye adsorbed onto AC adsorbent for a unit equilibrium concentration. When *1/n* ranges between 0 and 1, the adsorption can be considered favorable and the surface is heterogeneous [38]. The plot of log q_e in the function of log C_e shown in Fig. 13 yielded straight lines with a slope '1/n'. The Freundlich constants (K_f and 1/n) are calculated and shown in Table 5. The values 1/n = 0.1309 for the AC600 and 1/n =0.0534 for the AC900 can be interpreted as indicators of the existence of favorable adsorption and heterogeneous surfaces.

The Dubinin-Radushkevich isotherm model is generally applied to express the adsorption mechanism with Gaussian energy distribution on a heterogeneous surface [39] and calculated in function of Equations (8), (9), and (10).

$$q_e = q_s e^{-\beta\varepsilon^2} \quad (8)$$

$$\ln q_e = \ln q_s - \beta\varepsilon^2 \quad (9)$$

$$\varepsilon = RT \ln(1 + \frac{1}{C_e}) \quad (10)$$

Where q_e is the amount of adsorbate in the adsorbent at equilibrium (mg/g), q_s is the theoretical isotherm saturation capacity (mg/g), β is the Dubinin-Radushkevich isotherm constant (mol^2/kJ^2), R is the gas constant (8.314 J/mol K), T is the absolute temperature (K), and C_e is the absorbate equilibrium concentration (mg/L).

The approach that was usually applied to distinguish the physical and chemical adsorption was the mean free energy, E computed according to Eq. (11).

$$E = \frac{1}{\sqrt{2\beta}} \quad (11)$$

Figs. 14 and 15 exhibit the linear plot of Dubinin-Radushkevich Ln(q_e) in the function of (ε^2), of removal of IC by AC600 and AC900, respectively. These figures show that the mean free energy E was 0.11 kJ/mol for AC600 adsorption and 0.79 kJ/mol for AC900 adsorption, indicating that the adsorption of IC on activated carbon from the leaves of *agave Americana L* was a physisorption process.

The parameters obtained for the Langmuir, Freundlich, and Dubinin–Radushkevich models are presented in Table 5. In this study, Langmuir appeared to be very consistent because the correlation factors (R^2) were the highest. The result showed that the maximum adsorption capacity obtained with the AC900 was better than or comparable to those obtained with the AC600.

Thermodynamics study

The final result of this study was related to the nature

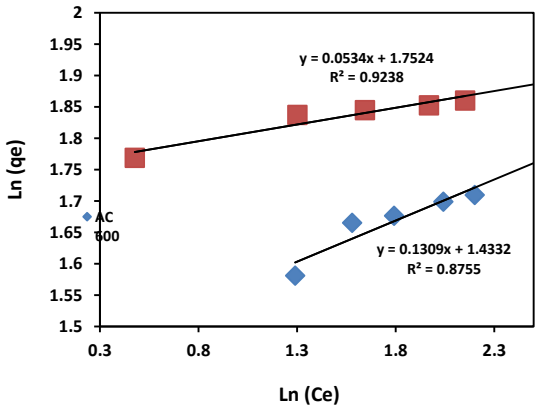

Fig. 13: Freundlich Isotherm model for removal of IC by AC600 and AC900 (pH=3.0, T= 25 °C, C_0=50 mg/L).

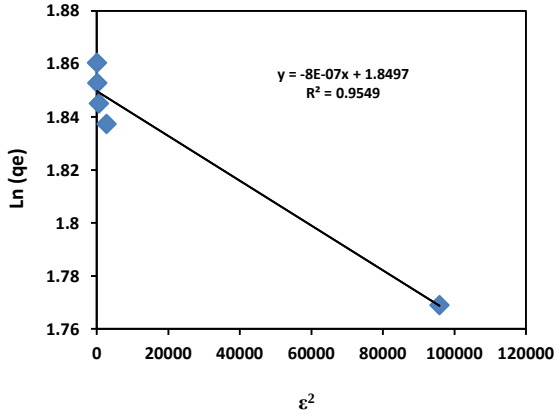

Fig. 14: Dubinin–Radushkevich Isotherm model for removal of IC by AC900 (pH=3.0, T= 25 °C, C_0=50 mg/L).

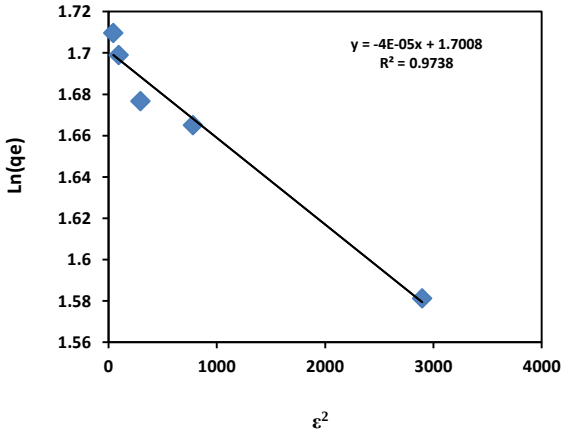

Fig. 15: Dubinin–Radushkevich Isotherm model for removal of IC by AC 600 (pH=3.0, T= 25 °C, C_0=50 mg/L).

of the adsorption of IC on AC from the *Agave Americana L*. The parameters of the thermodynamics analysis were the free energy change ΔG°, enthalpy change ΔH°, and entropy change ΔS°. The free energy change ΔG° is given by

$$\Delta G^0 = -RTlnK_c \quad (12)$$

Where $\Delta G°$ is the free energy change (kJ/mol); R is the universal gas constant (8.314 J/mol K); T is the absolute temperature (K); K_c is the distribution coefficient (L/g) [29] calculated in function of equation (13) below

$$K_c = \frac{q_e}{C_e} \quad (13)$$

According to the fundamental thermodynamic equation (14) and the van't Hoff equation (15)

$$\Delta G^0 = \Delta H^0 - T\Delta S^0 \quad (14)$$

$$ln(\rho K_c) = -\frac{\Delta H^0}{RT} + \frac{\Delta S^0}{R} \quad (15)$$

The plot of Ln(ρK_c) versus (1/T) makes it possible to deduce ΔH° and ΔS° [40]. ρ is the water density.

For AC600 the free energy ΔG° value ranged between -8 and -9 kJ/mol for temperatures ranging between 298 and 318 K. Similarly, for AC900, the free energy ΔG° value ranged between -10 and -12 kJ/mol for temperatures ranging between 298 and 318 K, respectively (Fig.16). In line with *Lin et al.* [41], this would indicate that the adsorption was a spontaneous physisorption process. The positive value of enthalpy (19.30 kJ/mol) shows that the adsorption of IC on AC900 is endothermic. The positive value of entropy ΔS° (100.13 J/mol K) would be an indicator of the random change between the liquid and solid interface. The Thermodynamic parameters of AC600 and AC 900 adsorption are represented in Table 6.

Comparative study

According to the theoretical q_0 calculated by the Langmuir model, AC600 and AC900 had a dye maximum adsorption capacity compared to the results obtained with various activated carbons prepared from different precursors and different activation procedures, as can be seen in Table 7.

CONCLUSIONS

This study attempted to show that the *Agave Americana L* leaves would be a potential source of a very effective AC. In addition to the chemical activation of the

Table 5: Langumir, Freundlich and Dubinin–Radushkevich isotherms of IC adsorption on the AC600 and the AC900.

AC	Langmuir model				Freundlich model			Dubinin – Radushkevich model		
	q_0 (mg/g)	b	R_l (L/mg)	R^2	1/n	K_f (mg/g) $(L/mg)^{1/n}$	R^2	E(kJ/mol)	q_s (mg/g)	R^2
AC600	43.66	0.10	0.16	0.99	0.13	4.19	0.87	0.11	5.47	0.97
AC900	61.72	0.52	0.03	0.99	0.05	5.76	0.92	0.79	6.35	0.95

Table 7: Comparative study of maximum adsorption capacity of Indigo Carmine onto activated carbon.

Adsorbent	Maximum adsorption capacity (mg/g)	References
AC900	61.72	This study
AC600	43.66	This study
Layered Double Hydroxide	55.5	[31]
Chitin	5.78	[42]
Chitosan	71.82	[42]
Rice husk ash	65.90	[4]

Table 6: Thermodynamic parameters of AC600 and AC900 adsorption.

Activated carbon	Temperature (K)	ΔG° (kJ/mol)	ΔH° (kJ/mol)	ΔS° (J/mol K)
AC600	298	-8.151		
	308	-8.578	5.136	44.538
	318	-9.041		
AC900	298	-10.628		
	308	-11.446	19.303	100.133
	318	-12.637		

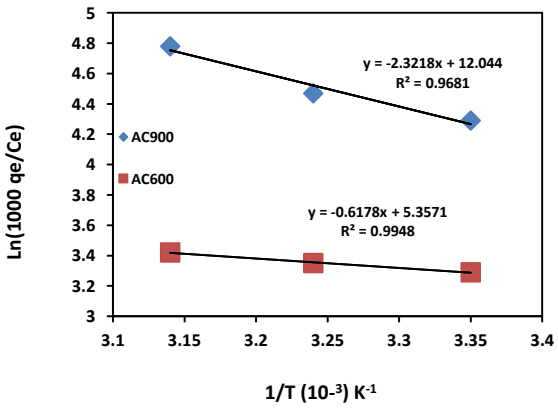

Fig. 16: Thermodynamic study for removal of IC by AC600 and AC900 (pH=3.0, C_0=50 mg/L).

Agave Americana L, this study revealed that the AC made from this plant was a porous structure with a surface area of 38 m²/g. This AC would have a maximum adsorption capacity of 61.72 mg/g for IC. This would make it a promising carbon for filtering dyes from wastewaters. In addition, after a thorough review of the existing models of the adsorption process of IC on AC600 and AC900, this study adopted the Langmuir isotherm model. It revealed that the adsorption of IC is physisorption and endothermic in nature. Finally, the use of the *Agave Americana L* leaves to prepare the AC would be one way of valorizing this invasive and useless plant and reducing the cost of producing AC.

Table 7: Comparative study of maximum adsorption capacity of Indigo Carmine onto activated carbon.

Adsorbent	Maximum adsorption capacity (mg/g)	References
AC900	61.72	This study
AC600	43.66	This study
Layered Double Hydroxide	55.5	[31]
Chitin	5.78	[42]
Chitosan	71.82	[42]
Rice husk ash	65.90	[4]

Acknowledgment

The authors would like to thank Dr. Ayadi Hajji for proofreading, correcting the English, and improving the editing of the manuscript.

Received : Nov. 2, 2019 ; Accepted : May 5, 2020

REFERENCES

[1] Sahraei R., Cheraghi J., Hushmandfar R., Abbasi S., Mortazavi S. S., Noorizadeh H., Farmany A., Catalytic Oxidation of Indigo Carmine in the Presence of Silver Nanoparticles: Application to Groundwater Analysis, *J. Chinese Chem. Soc.*, **60**: 195-198 (2013).

[2] Sari M. M., Removal of Acidic Indigo Carmine Textile Dye from Aqueous Solutions Using Radiation Induced Cationic Hydrogels, *Water Sci. Technol.*, **61(8)**: 2097–2104 (2010).

[3] Mittal A., Mittal J., Kurup L., Utilization of Hen Feathers for the Adsorption of Indigo Carmine from Simulated Effluents, *JEPS*, **1**: 92-100(2007).

[4] Arenas C. N., Vasco A., Betancur M., Martinez J. D., Removal of Indigo Carmine (IC) from Aqueous Solution by Adsorption through Abrasive Spherical Materials Made of Rice Husk Ash (RHA), *Proc. Saf. Env. Prot.*, **106**: 224-238 (2017).

[5] Almoisheer N., Alseroury F. A., Kumar R., Aslam M., Barakat M. A., Adsorption and Anion Exchange Insight of Indigo Carmine onto CuAl-LDH/SWCNTs Nanocomposite: Kinetic, Thermodynamic and Isotherm Analysis, *RSC Adv.*, **9**: 560–568 (2019).

[6] Lakshmi U.R., Srivastava V.C., Mall I.D., Lataye D.H., Rice Husk Ash as an Effective Adsorbent: Evaluation of Adsorptive Characteristics for Indigo Carmine Dye, *J. Env. Management.*, **90**: 710-720 (2009).

[7] Yousefpour M., Modelling of Adsorption of Zinc and Silver Ions on Analcime and Modified Analcime Zeolites Using Central Composite Design, *Iran. J. Chem. Chem. Eng. (IJCCE)*, **36(4)**: 81–90 (2017).

[8] Ferhat D., Nibou D., Elhadj M., Amokrane S., Adsorption of Ni^{2+} Ions onto NaX and NaY zeolites: Equilibrium, Kinetics, Intra Crystalline Diffusion and Thermodynamic Studies, *Iran. J. Chem. Chem. Eng. (IJCCE)*, **38(6)**: 63–81 (2019).

[9] Ba S., Ennaciri K., Yaacoubi A., Alagui A., Bacaoui A., Activated Carbon from Olive Wastes as an Adsorbent for Chromium Ions Removal, *Iran. J. Chem. Chem. Eng. (IJCCE)*, **37(6)**: 107-123 (2018).

[10] Ben Nasr J., Hamdi N., Elhalouani F., Characterization of Activated Carbon Prepared from Sludge Paper for Methylene Blue Adsorption, *J. Mater. Env. Sci.*, **8**: 1960-1967 (2017).

[11] Bohli T., Ouederni A., Villaescusa I., Simultaneous Adsorption Behavior of Heavy Metals onto Microporous Olive Stones Activated Carbon : Analysis of Metal Interactions, *Euro-Mediterranean J. Environ. Integr.*, **2(1)**: 1–15 (2017).

[12] Demirbas A., Heavy Metal Adsorption onto Agro-Based Waste Materials: A Review. *J. Hazard. Mater.*, **157 (2–3)**: 220–229 (2008).

[13] Piai L., Blokland M., van der Wal A., Langenhoff A., Biodegradation And Adsorption of Micropollutants by Biological Activated Carbon from a Drinking Water Production Plant, *J. Hazard. Mater.*, **388**: (2020).

[14] Esmaeili A., Ghasemi S., Zamani F., Investigation of Cr(VI) Adsorption by Dried Brown Algae Sargassum sp. and Its Activated Carbon. *Iran. J. Chem. Chem. Eng. (IJCCE)*, **31(4)**: 11–19 (2012).

[15] Crini G., Non-Conventional Low-Cost Adsorbents for Dye Removal: A Review, *Bioresource Technology*, **97**: 1061–1085 (2006).

[16] Tsai W. T., Chang C. Y., Lin M. C., Chien S. F., Sun H. F., Hsieh M. F., Adsorption of Acid Dye onto Activated Carbon Prepared from Agricultural Waste Bagasse by $ZnCl_2$ Activation, *Chemosphere,* **45**: 51–58 (2001).

[17] Spessato L., Bedin K. C., Cazetta A. L., Souza I. P. A. F., Duarte V. A., Crespo L. H. S., Silva M. C., Pontes R. M., Almeida V., KOH-Super Activated Carbon from Biomass Waste: Insights into the Paracetamol Adsorption Mechanism and Thermal Regeneration Cycles, *J. Hazard. Mater.* , **371**: 499–505 (2019).

[18] Kazemipour M., Ansari M., Tajrobehkar S., Removal of Lead, Cadmium, Zinc, and Copper from Industrial Wastewater by Carbon Developed from Walnut, Hazelnut, Almond, Pistachio Shell, and Apricot Stone. *J. Hazard. Mater.*, **150(2)**: 322–327 (2008).

[19] Mondal M. K., Garg R., A comprehensive Review on Removal of Arsenic Using Activated Carbon Prepared from Easily Available Waste Materials. *Environ. Sci. Pollut. Res.*, **24(15)**: 13295–13306 (2017).

[20] Heidarinejad Z., Dehghani M. H., Heidari M., Javedan G., Ali I., Sillanpää M., Methods for Preparation and Activation of Activated Carbon: A Review, *Environ. Chem. Lett.*, **18**: 393–415 (2020).

[21] Mansouri A., Ben Nasr J., Ben Amar M., Elhalouani F., Characterization of Fiber Extracted from Agave americana after Burial in Soil. Fibers and Polymers, **21(4)**: 724-732 (2020).

[22] Bezazi A., Belaadi A., Bourchak M., Scarpa F., Boba K., Novel Extraction Techniques, Chemical and Mechanical Characterisation of Agave Americana L. Natural Fibres, *Composites Part B: Engineering*, **66**: 194–203 (2014).

[23] Maaloul N., Ben Arfi R., Rendueles M., Ghorbal A., Diaz M., Dialysis-Free Extraction and Characterization of Cellulose Crystals from Almond (Prunus Dulcis) Shells. *J. Mater. Environ. Sci.,* **8(11)**: 4171-4181 (2017).

[24] Ben Arfi R., Karoui S., Mougin K., Ghorbal A., Adsorptive Removal of Cationic and Anionic Dyes from Aqueous Solution by Utilizing Almond Shell as Bioadsorbent, *Euro-Mediterranean J. Environ. Integr.*, **2(1)**: 217-229 (2017).

[25] Ben Arfi R., Karoui S., Mougin K., Ghorbal A., Cetyltrimethylammonium Bromide-Treated Phragmites Australis Powder as Novel Polymeric Adsorbent for Hazardous Eriochrome Black T Removal from Aqueous Solutions, *Polym. Bull.*, **76(10)**: 5077–5102 (2019).

[26] Maaloul N., Oulego P., Rendueles M., Ghorbal A., Díaz M., Synthesis and Characterization Of Eco-Friendly Cellulose Beads for Copper (II) Removal from Aqueous Solutions, *Environ. Sci. Pollut. Res.*, **27**: 23447–23463 (2020).

[27] Maaloul N., Oulego P., Rendueles M., Ghorbal A., Díaz M., Novel Biosorbents from Almond Shells: Characterization and Adsorption Properties Modeling for Cu(II) Ions from Aqueous Solutions. *J. Environ. Chem. Eng.*, **5(3)**: 2944–2954 (2017).

[28] Lahouioui M., Ben Arfi R., Fois M., Ibos L., Ghorbal A., Investigation of Fiber Surface Treatment Effect on Thermal, Mechanical and Acoustical Properties of Date Palm Fiber-Reinforced Cementitious Composites. *Waste and Biomass Valorization*, 11: 4441–4455 (2020).

[29] Karoui S., Ben Arfi R., Mougin K., Ghorbal A., Assadi A.A., Amrane A., Synthesis of novel Biocomposite Powder For Simultaneous Removal of Hazardous Ciprofloxacin and Methylene Blue: Central Composite Design, Kinetic and Isotherm Studies Using Brouers-Sotolongo Family Models, *J. Hazard. Mater.*, **387**: 121675 (2020).

[30] Yagmur E., Gokce Y., Tekin S., Semerci N.I., Aktas Z., Characteristics and Comparison of Activated Carbons Prepared from Oleaster (Elaeagnus Angustifolia L.) Fruit Using KOH and $ZnCl_2$. *Fuel*, **267**: 117232 (2020).

[31] Ahmed, M.A., Brick, A.A., Mohamed, A.A., An Efficient Adsorption of Indigo Carmine Dye from Aqueous Solution on Mesoporous Mg/Fe Layered Double Hydroxide Nanoparticles Prepared by Controlled Sol-Gel Route, *Chemosph.*, **174**: 280-288 (2017).

[32] Pezoti Junior O., Cazetta A. L., Gomes R. C., Barizão É. O., Souza I.P.A.F., Martins AC., Asefa T., Almeida V.C., Synthesis of $ZnCl_2$-Activated Carbon from Macadamia Nut Endocarp (Macadamia integrifolia) by Microwave-Assisted Pyrolysis: Optimization Tsing RSM and Methylene Blue Adsorption. *J. Anal. Appl. Pyrolysis*, **105**: 166–176 (2014).

[33] Deng H., Yang L., Tao G., Dai J., Preparation and Characterization of Activated Carbon from Cotton stalk by Microwave-Assisted Chemical Activation-Application in Methylene Blue Adsorption from Aqueous Solution. *J. Hazard. Mater.*, **166(2–3)**: 1514–1521 (2009).

[34] Rejeb R., Antonissen G., De Boevre M., Detavernier C.C., Van de Velde M., De Saeger S., Ducatelle R., Hadj Ayed M., Ghorbal A., Calcination Enhances the Aflatoxin and Zearalenone Binding Efficiency of a Tunisian Clay. *Toxins (Basel).* **11(10)**: 602 (2019).

[35] Repo E., Warchol J.K., Kurniawan T.A., Sillanp M.E.T., Adsorption of Co(II) and Ni(II) by EDTA- and/or DTPA-Modified Chitosan: Kinetic and Equilibrium Modeling. *Chem. Eng. J.*, **161(1–2)**: 73–82 (2010).

[36] Repo E., Kurniawan T.A., Warchol J.K., Sillanp M. E.T., Removal of Co(II) and Ni(II) Ions from Contaminated Water using Silica Gel Functionalized with EDTA and/or DTPA as Chelating Agents. *J. Hazard. Mater.*, **171(1–3):** 1071–1080 (2009).

[37] Malik P.K., Dye removal from Wastewater Using Activated Carbon Developed from Sawdust; Adsorption Equilibrium and Kinetics, *J. Hazard. Mater*., **113**: 81-88 (2004).

[38] Namasivayam C., Kavitha D., Removal of Congo Red from Water by Adsorption onto Activated Carbon Prepared from Coir Pith, an AgriculturalSolid Waste, *Dyes Pigment*, **54**: 47-58 (2002).

[39] Hobson J. P., Physical adsorption isotherms extending from ultrahigh vacuum to vapor pressure. *J. Phys. Chem.*, **73(8)**: 2720–2727 (1969).

[40] Zhang Z., Moghaddam L., O'Hara I. M., Doherty W.O.S., Congo Red Adsorption by Ball-Milled Sugarcane Bagasse. *Chem. Eng. J.*,**178**: 122–128 (2011).

[41] Lin K., Pan J., Chen Y., Cheng R., Xu X., Study the Adsorption of Phenol from Aqueous Solution on Hydroxyapatite Nanopowders. *J. Hazard. Mater.*, **161(1)**: 231–240 (2009).

[42] Prado, A.G.S., Torres, J.D., Faria, E.A., Dias, S.C.L., Comparative Adsorption Studies of Indigo Carmine Dye on Chitin and Chitosan, *J. Coll. Interf. Sci.*, **277**: 43–47 (2004).